A Tractography Analysis of Two Deep Brain Stimulation White Matter Targets for Depression

David A. Gutman, Paul E. Holtzheimer, Timothy E. J. Behrens, Heidi Johansen-Berg, and Helen S. Mayberg

Background: Deep brain stimulation (DBS) of the subcallosal cingulate white matter (SCCwm) or anterior limb of the internal capsule (ALIC) may be effective in treating depression. Connectivity patterns of these regions may inform on mechanisms of action for DBS of these targets.

Methods: Diffusion tensor imaging (DTI) and probabilistic tractography were performed in 13 nondepressed subjects to determine connectivity patterns of SCCwm and ALIC. Tract maps were generated for each target in each subject, and tract voxels were coded as being unique to either target or shared. Group level tract maps were generated by including only those voxels common to at least 10 of 13 (>75%) subjects.

Results: The two targets have distinct patterns of connectivity with regions of overlap. The SCCwm showed consistent ipsilateral connections to the medial frontal cortex, the full extent of the anterior and posterior cingulate, medial temporal lobe, dorsal medial thalamus, hypothalamus, nucleus accumbens, and the dorsal brainstem. The ALIC seed, in contrast, demonstrated widespread projections to frontal pole, medial temporal lobe, cerebellum, nucleus accumbens, thalamus, hypothalamus, and brainstem. Common to both targets, albeit through distinct white matter bundles, were connections to frontal pole, medial temporal lobe, nucleus accumbens, dorsal thalamus, and hypothalamus.

Conclusions: Connectivity patterns of these two DBS white matter targets suggest distinct neural networks with areas of overlap in regions implicated in depression and antidepressant response.

Key Words: DBS, deep brain stimulation, depression, diffusion tensor imaging, DTI, internal capsule, subgenual cingulate, tractography

Deep brain stimulation (DBS) is currently being tested as a potential treatment for severe, treatment-resistant depression (TRD) (1–4). A previous open-label study reported a 60% 6-month response rate with chronic DBS of the subcallosal cingulate white matter (SCCwm) (3,4). Acute and chronic antidepressant effects have also been reported with stimulation of other white matter targets, including the ventral most aspect of the anterior limb of the internal capsule (ALIC) (2,5–7) and the inferior thalamic peduncle (8), as well as gray matter targets, including the globus pallidus internus (9) and nucleus accumbens (10).

It is hypothesized that DBS and other directed brain stimulation therapies (e.g., vagus nerve stimulation and repetitive transcranial magnetic stimulation) exert antidepressant effects via modulation of activity within neural networks responsible for regulating mood and associated cognitive, circadian, and motor functions (11–15). Delineation of these networks is not only important for a better understanding of depression pathophysiology but also critical to the refinement and optimization of targeting for DBS and other brain stimulation therapies.

This issue mirrors that previously addressed in the development of DBS for movement disorders where motor circuit characterization directly led to evidence-based selection of several potential DBS targets (7,16,17). Based on clinical trials resulting from this work, stimulation of both the internal globus pallidus and subthalamic nucleus are now standard treatments for intractable motor symptoms in Parkinson's disease (17), albeit with different side effect profiles (7,18,19).

Compared with the neural systems underlying motor control, where the anatomical and physiological connections of key regions are well-characterized, the neural circuitry involved in depression is less well understood. However, extensive neuroimaging and neuropathological data consistently implicate a common set of cortical and subcortical regions in the regulation of normal and abnormal mood states (20,21). Based on these data, putative depression models have emerged (22) with the structural validity for these models derived largely from nonhuman primate tract tracing (23–29). Examining the structural validity of these models in human subjects has obvious practical implications for the development and refinement of brain stimulation therapies including differential safety and efficacy.

Diffusion tensor imaging (DTI) is a magnetic resonance imaging technique that exploits the directional dependent diffusion of water molecules in brain white matter, with the principal diffusion direction corresponding to the predominant direction in oriented fiber bundles (30). By modeling local diffusion properties, it is possible to estimate these directions and to follow them using probabilistic tractography (31). This method has previously been used to characterize the connectivity of subcortical (31,32) and brainstem structures (33,34), as well as cortical areas (35,36), including prefrontal and anterior cingulate cortices (37,38). Pathways traced in this way are reproducible (39) and generally match those identified using postmortem dissection or primate tract tracing (37,40). Recent advances in modeling of local diffusion properties allow estimation of more than one fiber direction at each voxel, enabling tracing of crossing fibers (41); this is of particular benefit when studying cingulate anatomy, as pathways to and from the cingulate cortex tend to be difficult to trace given the proximity of the corpus callosum and cingulum bundle.

From the Department of Psychiatry and Behavioral Sciences (DAG, PEH, HSM), Emory University School of Medicine, Atlanta, Georgia; and Centre for Functional MRI of the Brain (TEJB, HJ-B) and Department of Experimental Psychology (TEJB), University of Oxford, Oxford, United Kingdom.

Address reprint requests to David A. Gutman, M.D., Ph.D., Department of Psychiatry and Behavioral Sciences, Emory University School of Medicine, 101 Woodruff Circle, Suite 4000 WMRB, Atlanta, GA 30322; E-mail: dgutman@emory.edu.

Received May 16, 2008; revised September 16, 2008; accepted September 19, 2008.

0006-3223/09/$36.00
doi:10.1016/j.biopsych.2008.09.021

We have previously examined variability along the full extent of the subcallosal and pregenual white matter region to determine variability in connectivity in and around our primary DBS depression study target (42). In the present study, the structural connectivity (derived from probabilistic tractography of DTI data) of this subcallosal target was compared with that of a second target being investigated for TRD, specifically the ventral aspect of the ALIC (2,5).

Methods and Materials

1.5 Tesla DTI Acquisition

Diffusion-weighted images were acquired in 13 healthy subjects (72 × 2 mm thick axial slices, matrix 128 × 104, field of view 256 × 208 mm, giving a voxel size of 2 × 2 × 2 mm) (9 male subjects, 4 female subjects, aged 20 to 36, mean age ~26.7 ± 5.2 years) using a 1.5 tesla (T) Siemens Sonata scanner (Siemens AG, Malvern, Pennsylvania) with maximum gradient strength of 40 mTm^{-1}. The diffusion weighting was isotropically distributed along 60 directions using a b-value of 1000 smm^{-2}. A T1-weighted anatomical image was acquired for each subject using a three-dimensional (3-D) fast low-angle shot (FLASH) sequence (repetition time = 12 msec, echo time = 5.65 msec, and flip angle = 19°, with elliptical sampling of k-space, giving a voxel size of 1 × 1 × 1 mm in 5 min and 5 sec). All subjects were right-handed, with no history of psychiatric or neurological disease. Informed written consent was obtained from all subjects in accordance with ethical approval from the Central Office for Research Ethics Committees, United Kingdom.

Diffusion Image Analysis

Diffusion images were processed using Functional MRI of the Brain's Diffusion Toolbox (FDT) (www.fmrib.ox.ac.uk/fsl; Analysis Group, FMRIB, Oxford, United Kingdom) (43,44). First, diffusion-weighted, T1-weighted, and Montreal Neurological Institute (MNI) standard brain template images (45) were skull-stripped (46), followed by affine registration (47) to derive transformation matrices among the three spaces. Next, a multifiber diffusion model (41) was fitted that estimates probability distributions of the direction of fiber populations passing through each brain voxel. For each probabilistic diffusion tensor imaging tractography run, 25,000 streamline samples were generated from each seed voxel to build up a connectivity distribution. The number of these samples passing through each brain voxel was interpreted as proportional to the probability of the connection to the seed voxel. By fitting a multifiber model to the diffusion data, pathways were traced through regions of fiber crossing (41).

Figure 1. Mean connectivity maps for seeds in the SCCwm **(A)** (in blue) and ALIC **(B)** (in red). The ROIs used for the targets are displayed in the first row. Population-based mean tractography maps indicate voxels common to at least 75% of subjects. ALIC, anterior limb of the internal capsule; R, right; ROI, region of interest; SCCwm, subcallosal cingulate white matter.

Region of Interest Selection

Seed masks (Figure 1A and 1B, top row) were generated based on the two published white matter DBS targets for depression (3,5). All regions of interest (ROIs) were drawn in Montreal Neurological Institute standard space (voxel dimension 2 mm × 2 mm × 2 mm/total voxel volume of 8 mm^3). For the SCCwm target, a right and left 3 × 3 × 1 voxel ROI (volume = 72 mm^3 per ROI) was drawn on a single parasagittal image plane. The coordinates for the center of the SCCwm ROI were × = ±6, y = +26, z = −10, as previously described (3) (Figure 1A, column 1). For the ALIC target, 3 × 3 × 1 voxel ROIs were drawn in the coronal plane, just anterior to the anterior commissure, with the center of each ROI having coordinates of × = ±12, y = +6, and z = −4 mm, as described by Greenberg *et al.* (5). While the ROIs were drawn on different planes (axial vs. coronal), the ROI sizes were identical for both targets. Left and right hemisphere ROIs were pooled for subsequent analyses.

Individual Probabilistic Tractography Maps

For both the SCCwm and ALIC targets, a total of 450,000 streamline samples (18 voxels × 25,000 streamline samples/voxel) were used to generate the corresponding tractography map for each subject. The output of the probabilistic tractography algorithm for a given subject is a map in MNI standard space where the value at each voxel corresponds to the numbers of streamlined samples passing through a given voxel, which is interpreted as proportional to the probability of a connection to the seed target voxel (41). For each seed target, the group-wise, whole brain streamline intensity map was analyzed to determine the robust mean intensity, which is a mean calculated using only those values that fall within the 5% and 95% areas under the intensity histogram. Each map was smoothed using a 4 mm Gaussian kernel and the resultant image was then further thresholded to exclude outliers, specifically those voxels whose streamline intensity was less than 1% of the robust mean. This

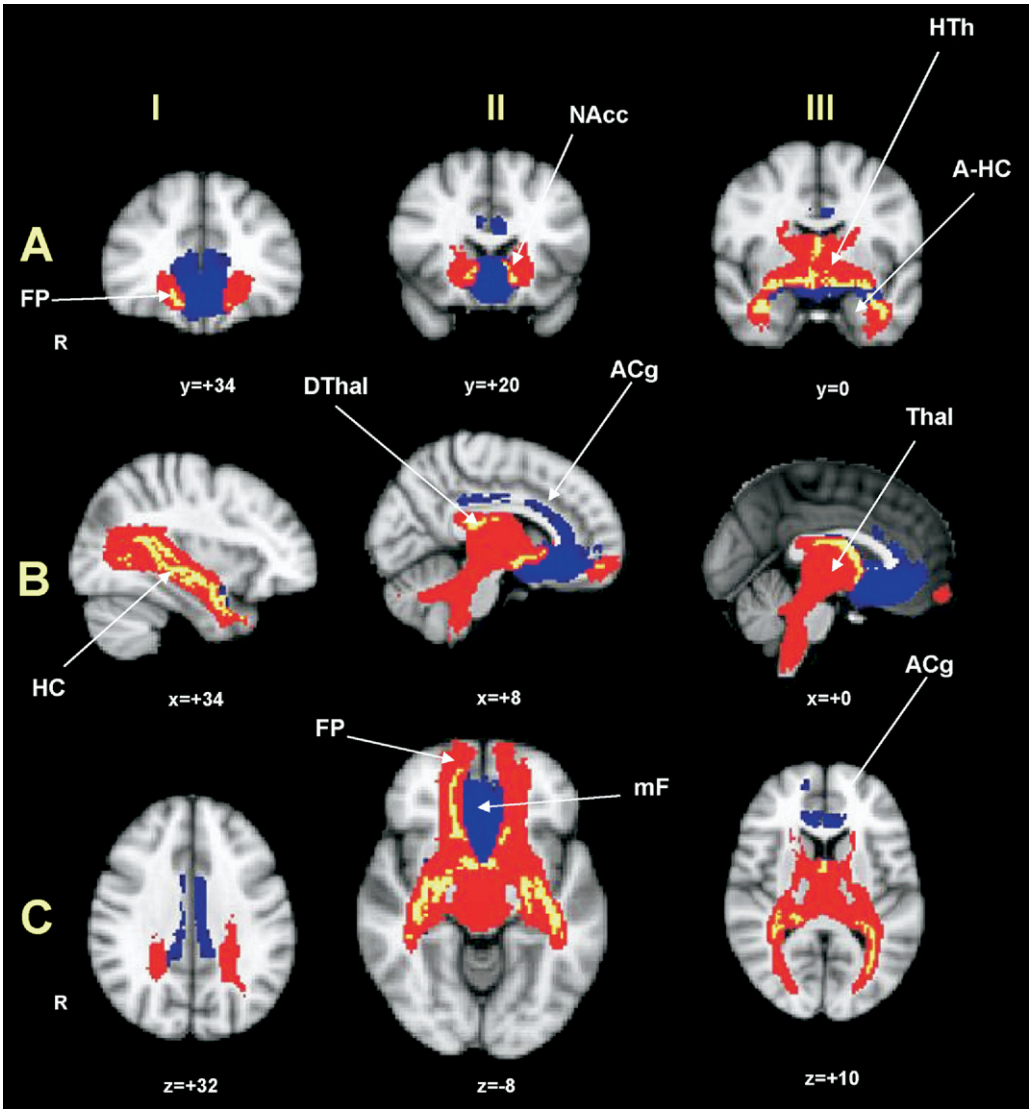

Figure 2. Unique and common projections for SCCwm and ALIC seeds. Areas of overlap (yellow) are superimposed on the mean tract maps for the SCCwm (blue) and ALIC (red). Areas of overlap indicate voxels shared by projections from both targets for at least 50% of subjects. ACg, anterior cingulate; A-HC, amygdala/hippocampus; ALIC, anterior limb of the internal capsule; DThal, dorsal thalamus; FP, frontal pole; HC, hippocampus; HTh, hypothalamus; mF, medial frontal cortex; NAcc, nucleus accumbens; R, right; SCCwm, subcallosal cingulate white matter.

method reduces the variability seen with the absolute global mean intensity that can be skewed by the presence of voxels with very low or very high connectivity values (48).

Population Based Mean Probability Maps

Population probability maps were next derived by overlapping the individual subject probability maps. To generate these mean probability maps, each subject's individual map, after thresholding, was binarized with a voxel assigned a value of either 0 or 1 based on whether or not any streamline samples passed through that voxel in space, thus removing all relative probability information. These individual binary maps were then combined to generate a mean population map. In this new mean map, the value at each voxel represented the number of subjects whose individual probability map shared this voxel. With this binary method, voxels with low connectivity scores that were consistent across subjects were retained. Lastly, this mean population map was thresholded to show voxels common to 75% or more of subjects.

Identification of Common Patterns of Connectivity Between Target Seeds

For each subject and each seed region, whole brain streamline intensity maps were generated as above and then thresholded to exclude outliers, specifically those voxels whose streamline intensity was less than 1% of the robust mean. Each individual's thresholded mean intensity map was then binarized (0 or 1 within a voxel). Lastly, contrasts were generated between these binarized maps to identify voxels both unique and common to the SCCwm and ALIC seeds across all subjects. Specifically, the binarized maps for each seed were summed, resulting in a map with voxels containing 0 (no streams with either target), 1 (unique to ALIC), 2 (unique to the SCCwm), or 3 (common to both targets).

Determination of Direct Connectivity Between SCCwm and ALIC

A final analysis was performed to determine whether a pathway could be traced between the two seeds. First, the SCCwm target was superimposed on the mean tractography map from the ALIC target and vice versa. Second, a restricted seed-to-target analysis, in which only fibers originating from within the seed region and passing through the target regions (in this case SCCwm to ALIC and vice versa) are identified, was performed to further determine the existence of a pathway between the two regions.

Results

Mean Connectivity of Each Target Seed

The SCCwm showed ipsilateral connections to medial frontal cortex, the full extent of the anterior and posterior cingulate, the anterior medial temporal lobe (amygdala-hippocampus), the dorsal medial thalamus, the hypothalamus, and nucleus accumbens (NAcc) (Figure 1A). Expected connections to the brainstem were not observed for the SCCwm in the mean connectivity maps; however, at the single subject level, distinct connections to the dorsal brainstem adjacent to the periaqueductal gray were observed in 12 of 13 subjects (see Supplement 1 for example images).

The ALIC seed, in contrast, demonstrated widespread and dense projections to the entire thalamus, hypothalamus and brainstem, frontal pole, medial temporal lobe (amygdala-hippocampus), cerebellum, and the NAcc (Figure 1B).

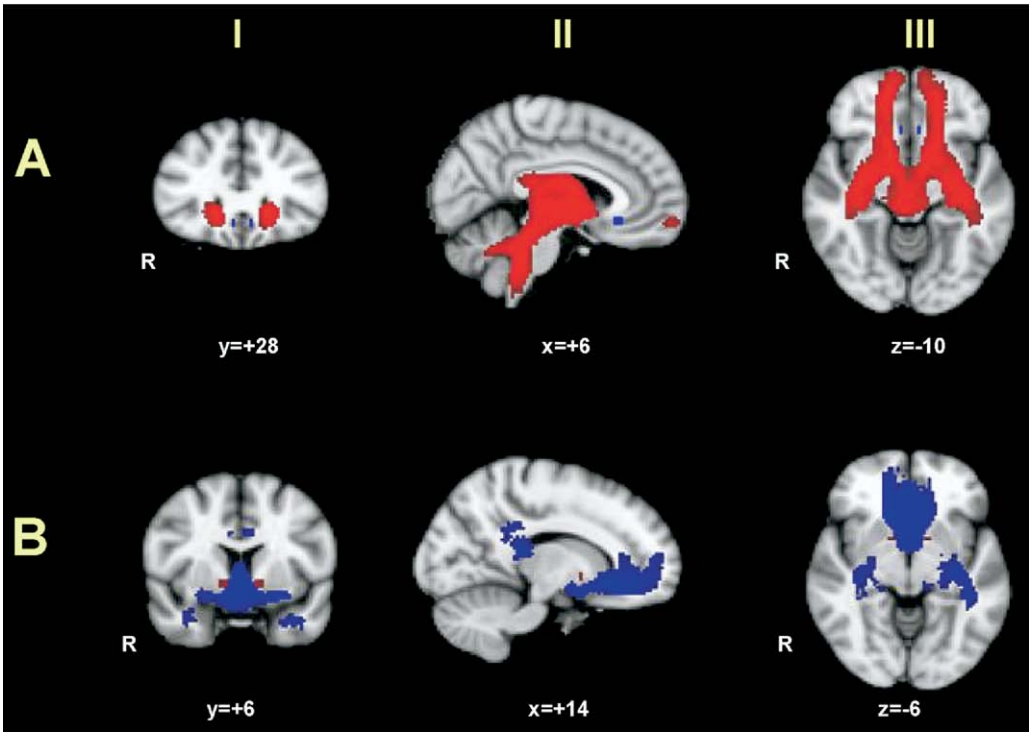

Figure 3. Seed locations relative to tract maps for each target. Row **(A)** shows the ALIC tract map (red) with the SCCwm seed superimposed (blue). Row **(B)** shows the SCCwm tract map (blue) with the ALIC seed superimposed (red). ALIC, anterior limb of the internal capsule; R, right; SCCwm, subcallosal cingulate white matter.

Common Connections for Each Target Seed

In general, the two seeds showed discrete connectivity patterns, with limited areas of overlap (Figure 2). Common to both targets were connections to the frontal pole (Figure 2 IIC), the amygdala/hippocampal complex (Figure 2 IIIA), hypothalamus, dorsal thalamus, and the NAcc. As the brainstem did not appear in the mean connectivity map for the SCCwm, this region did not appear in this contrast analysis (though, as described above, there are likely regions of overlap in the periaqueductal gray).

Despite these areas of overlap, the pattern of connectivity with these shared regions is largely divergent. For the frontal pole, the majority of fibers projecting from the SCCwm (in blue) travel primarily medially along the forceps minor, whereas the ALIC target fibers (in red) travel more laterally primarily via the anterior thalamic radiation (Figure 2 IIC). For the amygdala-hippocampal region, both appeared to send fibers through the medial temporal lobe within the uncinate fasciculus, though the apparent projections from the ALIC may represent commissural-hippocampal fibers adjacent to the ALIC (see Discussion). Both targets have connections to the NAcc and hypothalamus (Figure 2 IIB). Notable is that the ventral-most aspect of the ALIC abuts the caudal-most aspect of the nucleus accumbens. In contrast, the SCCwm connects predominantly to the rostral aspect of the NAcc. Both targets appear to share a common projection to the caudal aspect of the nucleus (in yellow, Figure 2 IIB).

Direct Connectivity Between ALIC and SCCwm

There was no overlap of either seed mean tract map with the other target seed (Figure 3). Further, the seed-target restricted analysis showed no connectivity between the two seed regions that was consistent between subjects.

Discussion

The primary aim of this study was to determine the patterns of connectivity of two white matter DBS targets currently being investigated for intractable major depression. These results indicate that the connectivity patterns of the SCCwm and ALIC are largely divergent but with some potentially important regions of overlap. Specifically, the SCCwm resides within a highly restricted medial-limbic-striatal network, while the ALIC target exists within a predominantly lateral cortical-thalamic-medial temporal network. Projections from both seeds overlap at the frontal pole, amygdala-hippocampal complex, nucleus accumbens, hypothalamus, dorsal thalamus, and dorsal brainstem, regions previously implicated in antidepressant response mechanisms (49–52).

Although both targets appear to project to some identical brain regions, differences in the trajectory of their respective pathways indicate likely differences in overall connectivity. Both targets connect to the frontal pole; however, the SCCwm projections follow a more medial route via the forceps minor, whereas the ALIC projections follow the more lateral anterior thalamic radiations. For the amygdala-hippocampal region, both targets connect to the medial temporal lobe within the uncinate fasciculus. Notably, detailed anatomical studies in nonhuman primates indicate there is no direct connection from the hippocampus to the ALIC target (53). However, commissural hippocampal fibers do ascend toward the anterior commissure and the base of the fornix, which are directly adjacent to the ventral aspect of the ALIC, likely accounting for the tractography results. Lastly, though both targets communicate directly to the NAcc, the most ventral part of the ALIC directly abuts the caudal aspect of the NAcc, while the SCCwm communicates along tracts terminating at the more rostral NAcc. Based on these combined differences, it seems reasonable to assume that these two white matter DBS targets each exist within separate neural networks (or subnetworks) that include common nodes (e.g., frontal pole, amygdala-hippocampus, dorsal thalamus, NAcc, hypothalamus, and dorsal brainstem).

Anatomically, these probabilistic tractography results are largely consistent with conventional tract-tracing studies performed in nonhuman primates. Tracer studies have shown that subcallosal gray matter regions (BA 25, 32, 24) have strong reciprocal cortical connections with orbitofrontal, dorsomedial prefrontal, and cingulate cortices (including pregenual, midcingulate, and posterior segments) (25,54) and more sparse connections to dorsolateral prefrontal cortex (23). Dense subcortical connections with the hypothalamus (55–57), ventral striatum (23,58–60), amygdala (56), and autonomic centers in the brainstem, including the periaqueductal gray, dorsal raphe, and locus coeruleus (56,61), have also been described. Functionally, areas of blood flow and metabolic changes with chronic DBS of the SCCwm in treatment-resistant depressed patients are seen in gray matter structures immediately adjacent to the tract terminations from the SCCwm seed in this study. This suggests expected concordance between anatomical and functional connectivity (3,22).

A reproducible connection from the SCCwm to the periaqueductal gray/brainstem was not identified across at least 75% of the subjects, despite the known presence of this connection based on nonhuman primate tract tracing (56,61). However, at a single subject level, SCCwm connections to the brainstem were discernible in 12 of 13 subjects (Supplement 1). Because the actual brainstem voxels showing the connection differed from subject to subject, this connection did not survive our more rigorous mean voxel-level thresholding.

Fewer tract studies in nonhuman primates have focused specifically on the connectivity of the ALIC. The connections seen with the ALIC target are consistent with previous reports of connections to the dorsolateral and ventrolateral prefrontal cortex. Recent studies examining fiber paths more specifically of the ALIC (23) reveal a much more complex pattern of connectivity, highly dependent on the rostral-caudal position within the ALIC, consistent with the expected afferents and efferents of the thalamus. Interestingly, we did not identify the predicted anterior cingulate connections with the ALIC target as previously shown in primates (23). Therefore, we examined subtle variations in ALIC connectivity immediately anterior and posterior to the primary ALIC ROI in a post hoc analysis. Fairly limited connections to the dorsal anterior cingulate were found ~4 mm medial to the initial target but with a more sparse distribution of fibers than seen with the SCCwm seed.

Several methodological limitations must be considered when interpreting these results. First, DTI-based tractography does not have the ability to distinguish between afferent and efferent pathways such that directionality of observed connections cannot be inferred. Therefore, identified patterns of connectivity must be viewed in context of known anatomical directionality analyses performed with specific anterograde and retrograde tracers. Second, there are no empirically validated guidelines on what should be considered a significant connection (i.e., what is the appropriate threshold of probability that should be used to determine a real connection from a spurious one); this limitation also accounts for how our method of thresholding may have underestimated common connections that were present when a less rigorous threshold was applied. Third, ROI size will clearly

influence the pattern of connectivity seen with probabilistic tractography. Although the relatively large ROI size in this study ($3 \times 3 \times 1$ voxels $= 6 \times 6 \times 2$ mm $= 72$ mm^3) is larger than either surgical target, this likely introduces little bias for the purposes of this study, since the area of effective stimulation from DBS would likely be at least this large (62). However, this relatively low resolution compared with ex vivo tract-tracing studies does not allow visualization of connections from specific neuronal populations to specific synaptic targets. This issue of resolution also likely accounts for difficulty in distinguishing the precise trajectory of tracts in and around the fornix, nucleus accumbens, dorsal thalamus, hypothalamus, and brainstem, where many converging but functionally distinct pathways likely reside within the same voxels.

Diffusion tensor imaging based tractography is a relatively new and evolving technique, and there is need for further validation studies. To date, there has been encouraging evidence that pathways identified using tractography agree with results based on postmortem dissection (63) and on tracer studies in nonhuman animals (64,65). However, there are situations in which tractography can identify spurious pathways or fail to trace pathways that are known to exist (64–66). Diffusion tensor imaging cannot currently achieve the level of resolution seen with classic anatomical methods. However, the overall pattern of connectivity can be compared, and DTI currently represents the best in vivo method currently available. For this reason, results from tractography should not be considered as equivalent to those from the gold standard techniques of tract tracing. Future validation studies, in which results from tractography are compared with those from invasive tracer studies across a range of different pathways, will help to clarify the limitations to this technique. However, the lack of ability to perform such detailed in vivo tract-tracing studies in humans hampers attempts to definitively validate DTI-based tractography results.

While larger clinical trials are needed to determine whether DBS at either of these targets is safe and efficacious for the treatment of depression, the current data suggest that these targets do not merely represent serial nodes in a common distributed circuit. Instead, these findings imply that antidepressant effects resulting from DBS at these two targets may be mediated through primary modulation of activity within two distinct neural networks or via secondary effects at regions where there are common connections (frontal pole, medial temporal lobe, dorsal thalamus, nucleus accumbens, hypothalamus, and/or dorsal brainstem). Shared and differential patterns of connectivity may also explain commonalities and differences in efficacy and side effect profiles of stimulation of these two targets, once comparable clinical data are available. Based on published reports, acute stimulation of the ALIC for obsessive-compulsive disorder and major depression reports voltage-dependent gustatory and olfactory sensations, autonomic changes (increased respiratory rate, nausea, sweating), and panic reactions (2,7); neither acute nor chronic SCCwm DBS in depressed patients have been associated with such effects (3,4).

By focusing on nondepressed control subjects, this study aimed to define the normal structural connectivity of putative neural networks implicated in depression and antidepressant response facilitated via DBS. Larger studies, including both control subjects and patients, as well as individualized tract analyses in single subjects, will help further clarify commonalities and variability within these networks in humans. Until in vivo methods for tract tracing are available for use in humans, it will be difficult to fully validate these techniques. However, the strong concordance with previous nonhuman primate findings suggests DTI-based probabilistic tractography will play a critical role in delineating these systems.

This work was supported by the United Kingdom Medical Research Council (TEJB), the Wellcome Trust (HJ-B), the Stanley Medical Research Institute (HSM), the Dana Foundation (HSM), the Woodruff Fund (HSM), a NARSAD Young Investigator Award (PEH), and K23 MH077869 (PEH).

HSM consults to Advanced Neuromodulation Systems (ANS; a division of St. Jude Medical) and has intellectual property rights on deep brain stimulation technology for treating depression that have been licensed to ANS. PEH consults to ANS, Tetragenex, Inc., and AstraZeneca, Inc. DAG, TEJB, and HJ-B have reported no biomedical financial interests or potential conflicts of interest.

Supplementary material cited in this article is available online.

1. Marangell LB, Martinez M, Jurdi RA, Zboyan H (2007): Neurostimulation therapies in depression: A review of new modalities. *Acta Psychiatr Scand* 116:174–181.
2. Malone DA, Dougherty DD, Rezai AR, Carpenter LL, Friehs GM, Eskander EN *et al.* (2008): Deep brain stimulation of the ventral capsule/ventral striatum for treatment-resistent depression [published online ahead of print October 9]. *Biol Psychiatry*.
3. Mayberg HS, Lozano AM, Voon V, McNeely HE, Seminowicz D, Hamani C, *et al.* (2005): Deep brain stimulation for treatment-resistant depression. *Neuron* 45:651–660.
4. Lozano AM, Mayberg HS, Giacobbe P, Hamani C, Craddock RC, Kennedy SH (2008): Subcallosal cingulate gyrus deep brain stimulation for treatment-resistant depression. *Biol Psychiatry* 64:461–467.
5. Greenberg BD, Malone DA, Friehs GM, Rezai AR, Kubu CS, Malloy PF, *et al.* (2006): Three-year outcomes in deep brain stimulation for highly resistant obsessive-compulsive disorder. *Neuropsychopharmacology* 31:2384–2393.
6. Nuttin B, Cosyns P, Demeulemeester H, Gybels J, Meyerson B (1999): Electrical stimulation in anterior limbs of internal capsules in patients with obsessive-compulsive disorder. *Lancet* 354:1526.
7. Okun MS, Mann G, Foote KD, Shapira NA, Bowers D, Springer U, *et al.* (2007): Deep brain stimulation in the internal capsule and nucleus accumbens region: Responses observed during active and sham programming. *J Neurol Neurosurg Psychiatry* 78:310–314.
8. Jimenez F, Velasco F, Salin-Pascual R, Hernandez JA, Velasco M, Criales JL, *et al.* (2005): A patient with a resistant major depression disorder treated with deep brain stimulation in the inferior thalamic peduncle. *Neurosurgery* 57:585–593.
9. Kosel M, Sturm V, Frick C, Lenartz D, Zeidler G, Brodesser D, *et al.* (2007): Mood improvement after deep brain stimulation of the internal globus pallidus for tardive dyskinesia in a patient suffering from major depression. *J Psychiatr Res* 41:801–803.
10. Schlaepfer TE, Cohen MX, Frick C, Kosel M, Brodesser D, Axmacher N, *et al.* (2008): Deep brain stimulation to reward circuitry alleviates anhedonia in refractory major depression. *Neuropsychopharmacology* 33:368–377.
11. Mayberg HS (2003): Positron emission tomography imaging in depression: A neural systems perspective. *Neuroimaging Clin N Am* 13:805–815.
12. Mayberg HS (2006): Defining neurocircuits in depression: Insight from functional neuroimaging studies of diverse treatments. *Psychiatr Ann* 36:259–268.
13. Mayberg HS, Brannan SK, Mahurin RK, Jerabek PA, Brickman JS, Tekell JL, *et al.* (1997): Cingulate function in depression: A potential predictor of treatment response. *Neuroreport* 8:1057–1061.
14. Mayberg HS (1997): Limbic-cortical dysregulation: A proposed model of depression. *J Neuropsychiatry Clin Neurosci* 9:471–481.
15. Dougherty DD, Rauch SL (2007): Somatic therapies for treatment-resistant depression: New neurotherapeutic interventions. *Psychiatr Clin North Am* 30:31–37.
16. Sakas DE, Panourias IG, Simpson BA (2007): An introduction to neural networks surgery, a field of neuromodulation which is based on advances in neural networks science and digitised brain imaging. *Acta Neurochir (Wien)* 97:3–13.
17. DeLong MR, Wichmann T (2007): Circuits and circuit disorders of the basal ganglia. *Arch Neurol* 64:20–24.

18. Appleby BS, Duggan PS, Regenberg A, Rabins PV (2007): Psychiatric and neuropsychiatric adverse events associated with deep brain stimulation: A meta-analysis of ten years' experience. *Mov Disord* 22:1722–1728.
19. Follett KA (2004): Comparison of pallidal and subthalamic deep brain stimulation for the treatment of levodopa-induced dyskinesias. *Neurosurg Focus* 17:E3.
20. Mayberg HS (2006): Defining neurocircuits in depression: Insights from functional neuroimaging studies of diverse treatments. *Psychiatr Ann* 36:258–266.
21. Dougherty DD, Rauch SL (2007): Brain correlates of antidepressant treatment outcome from neuroimaging studies in depression. *Psychiatr Clin North Am* 30:91–103.
22. Seminowicz DA, Mayberg HS, McIntosh AR, Goldapple K, Kennedy S, Segal Z, *et al.* (2004): Limbic-frontal circuitry in major depression: A path modeling meta-analysis. *Neuroimage* 22:409–418.
23. Haber SN, Kim KS, Mailly P, Calzavara R (2006): Reward-related cortical inputs define a large striatal region in primates that interface with associative cortical connections, providing a substrate for incentive-based learning. *J Neurosci* 26:8368–8376.
24. Petrides M, Pandya DN (2007): Efferent association pathways from the rostral prefrontal cortex in the macaque monkey. *J Neurosci* 27:11573–11586.
25. Carmichael ST, Price JL (1996): Connectional networks within the orbital and medial prefrontal cortex of macaque monkeys. *J Comp Neurol* 371:179–207.
26. Price JL, Carmichael ST, Drevets WC (1996): Networks related to the orbital and medial prefrontal cortex: A substrate for emotional behavior? *Prog Brain Res* 107:523–536.
27. Carmichael ST, Price JL (1995): Limbic connections of the orbital and medial prefrontal cortex in macaque monkeys. *J Comp Neurol* 363:615–641.
28. Ongur D, Ferry AT, Price JL (2003): Architectonic subdivision of the human orbital and medial prefrontal cortex. *J Comp Neurol* 460:425–449.
29. Ongur D, Price JL (2000): The organization of networks within the orbital and medial prefrontal cortex of rats, monkeys and humans. *Cereb Cortex* 10:206–219.
30. Beaulieu C, Allen PS (1994): Determinants of anisotropic water diffusion in nerves. *Magn Reson Med* 31:394–400.
31. Behrens TE, Johansen-Berg H, Woolrich MW, Smith SM, Wheeler-Kingshott CA, Boulby PA, *et al.* (2003): Non-invasive mapping of connections between human thalamus and cortex using diffusion imaging. *Nat Neurosci* 6:750–757.
32. Johansen-Berg H, Behrens TE, Sillery E, Ciccarelli O, Thompson AJ, Smith SM, *et al.* (2005): Functional-anatomical validation and individual variation of diffusion tractography-based segmentation of the human thalamus. *Cereb Cortex* 15:31–39.
33. Hadjipavlou G, Dunckley P, Behrens TE, Tracey I (2006): Determining anatomical connectivities between cortical and brainstem pain processing regions in humans: A diffusion tensor imaging study in healthy controls. *Pain* 123:169–178.
34. Sillery E, Bittar RG, Robson MD, Behrens TE, Stein J, Aziz TZ, *et al.* (2005): Connectivity of the human periventricular-periaqueductal gray region. *J Neurosurg* 103:1030–1034.
35. Rushworth MF, Behrens TE, Johansen-Berg H (2006): Connection patterns distinguish 3 regions of human parietal cortex. *Cereb Cortex* 16: 1418–1430.
36. Johansen-Berg H, Behrens TE, Robson MD, Drobnjak I, Rushworth MF, Brady JM, *et al.* (2004): Changes in connectivity profiles define functionally distinct regions in human medial frontal cortex. *Proc Natl Acad Sci U S A* 101:13335–13340.
37. Croxson PL, Johansen-Berg H, Behrens TE, Robson MD, Pinsk MA, Gross CG, *et al.* (2005): Quantitative investigation of connections of the prefrontal cortex in the human and macaque using probabilistic diffusion tractography. *J Neurosci* 25:8854–8866.
38. Anwander A, Tittgemeyer M, von Cramon DY, Friederici AD, Knosche TR (2007): Connectivity-based parcellation of Broca's area. *Cereb Cortex* 17:816–825.
39. Heiervang E, Behrens TE, Mackay CE, Robson MD, Johansen-Berg H (2006): Between session reproducibility and between subject variability of diffusion MR and tractography measures. *Neuroimage* 33:867–877.
40. Stieltjes B, Kaufmann WE, van Zijl PC, Fredericksen K, Pearlson GD, Solaiyappan M, *et al.* (2001): Diffusion tensor imaging and axonal tracking in the human brainstem. *Neuroimage* 14:723–735.
41. Behrens TE, Johansen-Berg H, Jbabdi S, Rushworth MF, Woolrich MW (2007): Probabilistic diffusion tractography with multiple fibre orientations: What can we gain? *Neuroimage* 34:144–155.
42. Johansen-Berg H, Gutman DA, Behrens TE, Matthews PM, Rushworth MF, Katz E, *et al.* (2008): Anatomical connectivity of the subgenual cingulate region targeted with deep brain stimulation for treatment-resistant depression. *Cereb Cortex* 18:1374–1383.
43. Smith SM, Jenkinson M, Woolrich MW, Beckmann CF, Behrens TE, Johansen-Berg H, *et al.* (2004): Advances in functional and structural MR image analysis and implementation as FSL. *Neuroimage* 23(suppl 1):S208–S219.
44. Behrens TEJ, Woolrich MW, Jenkinson M, Johansen-Berg H, Nunes RG, Clare S, *et al.* (2003): Characterization and propagation of uncertainty in diffusion-weighted MR imaging. *Magn Reson Med* 50:1077–1088.
45. Kennedy SH, Evans KR, Kruger S, Mayberg HS, Meyer JH, McCann S, *et al.* (2001): Changes in regional brain glucose metabolism measured with positron emission tomography after paroxetine treatment of major depression. *Am J Psychiatry* 158:899–905.
46. Smith SM (2002): Fast robust automated brain extraction. *Hum Brain Mapp* 17:143–155.
47. Jenkinson M, Smith SM (2001): Global optimisation for robust affine registration. *Med Image Anal* 5:143–156.
48. Ciccarelli O, Behrens TE, Altmann DR, Orrell RW, Howard RS, Johansen-Berg H, *et al.* (2006): Probabilistic diffusion tractography: A potential tool to assess the rate of disease progression in amyotrophic lateral sclerosis. *Brain* 129:1859–1871.
49. Tanis KQ, Newton SS, Duman RS (2007): Targeting neurotrophic/growth factor expression and signaling for antidepressant drug development. *CNS Neurol Disord Drug Targets* 6:151–160.
50. Pittenger C, Duman RS (2008): Stress, depression, and neuroplasticity: A convergence of mechanisms. *Neuropsychopharmacology* 33:88–109.
51. Airan RD, Meltzer LA, Roy M, Gong Y, Chen H, Deisseroth K (2007): High-speed imaging reveals neurophysiological links to behavior in an animal model of depression. *Science* 317:819–823.
52. Schlaepfer TE, Cohen MX, Frick C, Kosel M, Brodesser D, Axmacher N, *et al.* (2008): Deep brain stimulation to reward circuitry alleviates anhedonia in refractory major depression. *Neuropsychopharmacology* 33:368–377.
53. Schmahmann JD, Pandya DN (2006): *Fiber Pathways of the Brain*. New York: Oxford University Press.
54. Vogt BA, Pandya DN (1987): Cingulate cortex of the rhesus monkey: II. Cortical afferents. *J Comp Neurol* 262:271–289.
55. Barbas H, Saha S, Rempel-Clower N, Ghashghaei T (2003): Serial pathways from primate prefrontal cortex to autonomic areas may influence emotional expression. *BMC Neurosci* 4:25–37.
56. Freedman LJ, Insel TR, Smith Y (2000): Subcortical projections of area 25 (subgenual cortex) of the macaque monkey. *J Comp Neurol* 421:172–188.
57. Ongur D, An X, Price JL (1998): Prefrontal cortical projections to the hypothalamus in macaque monkeys. *J Comp Neurol* 401:480–505.
58. Kunishio K, Haber SN (1994): Primate cingulostriatal projection: Limbic striatal versus sensorimotor striatal input. *J Comp Neurol* 350:337–356.
59. Ferry AT, Ongur D, An X, Price JL (2000): Prefrontal cortical projections to the striatum in macaque monkeys: Evidence for an organization related to prefrontal networks. *J Comp Neurol* 425:447–470.
60. Haber SN, Kunishio K, Mizobuchi M, Lynd-Balta E (1995): The orbital and medial prefrontal circuit through the primate basal ganglia. *J Neurosci* 15:4851–4867.
61. An X, Bandler R, Ongur D, Price JL (1998): Prefrontal cortical projections to longitudinal columns in the midbrain periaqueductal gray in macaque monkeys. *J Comp Neurol* 401:455–479.
62. McIntyre CC, Miocinovic S, Butson CR (2007): Computational analysis of deep brain stimulation. *Expert Rev Med Devices* 4:615–622.
63. Stieltjes B, Kaufmann WE, van Zijl PC, Fredericksen K, Pearlson GD, Solaiyappan M, *et al.* (2001): Diffusion tensor imaging and axonal tracking in the human brainstem. *Neuroimage* 14:723–735.
64. Dyrby TB, Sogaard LV, Parker GJ, Alexander DC, Lind NM, Baare WF, *et al.* (2007): Validation of in vitro probabilistic tractography. *Neuroimage* 37:1267–1277.
65. Dauguet J, Peled S, Berezovskii V, Delzescaux T, Warfield SK, Born R, *et al.* (2007): Comparison of fiber tracts derived from in-vivo DTI tractography with 3D histological neural tract tracer reconstruction on a macaque brain. *Neuroimage* 37:530–538.
66. Pierpaoli C, Barnett A, Pajevic S, Chen R, Penix LR, Virta A, *et al.* (2001): Water diffusion changes in Wallerian degeneration and their dependence on white matter architecture. *Neuroimage* 13:1174–1185.